Propulsion and Power Research 2019;xxx(xxx):1−13

http://ppr.buaa.edu.cn/

Propulsion and Power Research

www.sciencedirect.com

ORGINAL ARTICLE

Cilia-assisted hydromagnetic pumping of biorheological couple stress fluids

K. Ramesh[a], D. Tripathi[b,*], O. Anwar Bég[c]

[a]Department of Mathematics, Symbiosis Institute of Technology, Symbiosis International University, Pune, 412115, India
[b]Department of Mechanical Engineering, Manipal University Jaipur, Rajasthan, 303007, India
[c]Fluid Mechanics/Propulsion, Aeronautical/Mechanical Engineering Department, Salford University, Manchester, UK

Received 19 December 2017; accepted 17 June 2018
Available online XXXX

KEYWORDS
Magneto hydrodynamics;
Metachronal waves;
Cilia;
Synchronous beating;
Polar couple stress fluid;
Physiological transport;
Magnetic blood pumps

Abstract A theoretical study is conducted for magnetohydrodynamic pumping of electro-conductive couple stress physiological liquids (e.g. blood) through a two-dimensional ciliated channel. A geometric model is employed for the cilia which are distributed at equal intervals and produce a whip-like motion under fluid interaction which obeys an elliptic trajectory. A metachronal wave is mobilized by the synchronous beating of cilia and the direction of wave propagation is parallel to the direction of fluid flow. A transverse static magnetic field is imposed transverse to the channel length. The Stokes' couple stress (polar) rheological model is utilized to characterize the liquid. The normalized two-dimensional conservation equations for mass, longitudinal and transverse momentum are reduced with lubrication approximations (long wavelength and low Reynolds number assumptions) and feature a fourth order linear derivative in axial velocity representing couple stress contribution. A coordinate transformation is employed to map the unsteady problem from the wave laboratory frame to a steady problem in the wave frame. No slip conditions are imposed at the channel walls. The emerging linearized boundary value problem is solved analytically and expressions presented for axial (longitudinal) velocity, volumetric flow rate, shear stress function and pressure rise. The flow is effectively controlled by three geometric parameters, viz cilia eccentricity parameter, wave

*Corresponding author.;
E-mail addresses: dharmtri@gmail.com, dtripathi@nituk.ac.in (D. Tripathi).
Peer review under responsibility of Beihang University.

Production and Hosting by Elsevier on behalf of KeAi

https://doi.org/10.1016/j.jppr.2018.06.002

number and cilia length and two physical parameters, namely magnetohydrodynamic (MHD) body force parameter and couple stress non-Newtonian parameter. Analytical solutions are numerically evaluated with MATLAB software. Axial velocity is observed to be enhanced in the core region with greater wave number whereas it is suppressed markedly with increasing cilia length, couple stress and magnetic parameters, with significant flattening of profiles with the latter two parameters. Axial pressure gradient is decreased with eccentricity parameter whereas it is elevated with cilia length, in the channel core region. Increasing couple stress and magnetic field parameter respectively enhance and suppress pressure gradient across the entire channel width. The pressure-flow rate relationship is confirmed to be inversely linear and pumping, free pumping and augmented pumping zones are all examined. Bolus trapping is also analyzed. The study is relevant to MHD biomimetic blood pumps.

Nomenclature

c	wave speed (unit: $m \cdot s^{-1}$)
a	mean width of the channel (unit: m)
λ	wavelength (unit: m)
t	time (unit: s)
ρ	density (unit: $kg \cdot m^{-3}$)
σ	electrical conductivity (unit: $S \cdot m^{-1}$)
B_0	magnetic field (unit: T)
μ	dynamic viscosity (unit: $kg \cdot m^{-1} \cdot s^{-1}$)
Θ	volume flow rate (unit: $m^3 \cdot s^{-1}$)
P	pressure (unit: Pa)
ϵ	cilia length parameter (unit: m)
U	longitudinal velocity (unit: $m \cdot s^{-1}$)
V	transverse velocity (unit: $m \cdot s^{-1}$)
α	measure of the eccentricity
$\bar{x}$	non-dimensional axial coordinate
$\bar{y}$	dimensionless transverse coordinate
$\bar{u}$	non-dimensional axial velocity
$\bar{v}$	dimensionless transverse velocity
$\bar{t}$	dimensionless time
$\bar{p}$	dimensionless pressure
β	wave number
Re	Reynolds number
γ	couple stress (polar) fluid parameter
M	Hartmann magnetic number
Q	dimensionless time-mean flow in the laboratory frame
F	dimensionless time-mean flow in the wave frame

1. Introduction

Ciliated propulsion arises in numerous physiological and biological systems. Cilia constitute small but intricate appendage structures which protrude from vessel walls. Cilia which average 10 μm in length can flex easily and assist therefore in many sophisticated transport mechanisms. They usually occur in high density arrays unlike flagella which usually appear in nature as single structures or pairs. Cilia beating mechanisms, which control the direction of induced thrust, therefore differ significantly from flagellar beating. They exhibit whip-like- motions and appear on cells, plants, physiological organs, marine organisms. They exert a substantial role across the biological spectrum and feature in for example physiology [1], respiration [2], embryonic mechano-transduction processes [3], coral reef systems [4], ventricular cerebrospinal fluid dynamics [5]. The beating mechanisms of cilia tend to be dominated by metachronal waves (these also dictate oscillations of flagella). The highly efficient energy usage of cilia has been documented in several studies including Gueron and Levit-Gurevich [6], Guirao and Joanny [7] and Vilfan and Julicher [8] in the latter, it has been shown that optimized performance is achieved by hydrodynamic interactions which result in synchronization of the cilia as nonlinear oscillators. The importance of cilia in sensory reception, mucociliary clearance and renal physiology disease has been addressed by Inés Ibañez-Tallon [9]. Brueckner [10] has examined the function of cilia in embryonic navigation.

The ciliated propulsion problem is attractive to fluid dynamics researchers since it is characterized by many geometric and viscous hydrodynamic features which are amenable to mathematical modelling. Historically the field of biological propulsion, specifically the fluid dynamics of a beating flagellum, was initiated in the early 1950s by Taylor (as lucidly reviewed in Lighthill [11]) who approximated the locomotion induced on a body by a tail beating in a regular manner in a Newtonian viscous medium. He derived an approximate relation connecting the organism velocity to the tail wave propagation speed. More recently there has been a considerable resurgence in interest in ciliated hydrodynamics, largely motivated by the emerging areas of biomimetics and bio-inspired engineering systems. Generally the approaches for simulating ciliated flows fall into two broad categories. The first has become known as the envelope model (followed in the current article) and the second is the sub-layer model. In the envelope model the cilia are densely packed and the engulfing fluid medium interacts with a waving material surface enveloping the top of the layer. Further sub-categories of the envelop approach feature models of an actively driven semi-flexible filament (this

aims to recreate actual cilia beat mechanisms) and beat shapes optimized based on pumping efficiency. A good perspective of many different approaches to ciliated hydrodynamics has been provided by Elgeti and Gompper [12]. Modern efforts have included both theoretical and computational analyses. Dauptain et al. [13] presented two-dimensional direct numerical simulation (DNS) results for hydrodynamics of regular oscillating flexible cilia arrays (ctenophore Pleurobrachia pileus), noting that power utilized is enhanced with cilia beating frequency, in consistency with actual behaviour reported in laboratory testing. Vilfan and Jülicher [14] presented computational simulations of flow fields produced by single and dual beating cilia configurations, studying carefully the development of synchronized states occur as a function of distance of cilia and relative beat orientation. Yang et al. [15] presented a numerical analysis of an unsteady viscous hydrodynamics for an individual elastic cilium by linking the internal force generation with the surrounding fluid as a simulation of multi-ciliary interaction in ovum transport in the oviduct and also mucus migration in the trachea. They showed that hydrodynamic coupling does lead to both synchrony and metachrony. Further investigations include the works of Dillon et al. [16] and Dresdner et al. [17].

The above investigations have invariably considered the biological fluid medium to be Newtonian i.e. they have ignored rheological effects. It is now firmly established for many decades that the vast majority of physiological media are characterized by substantial non-Newtonian properties. Accurate simulations therefore require non-Newtonian models. These models may be classified as biorheological models [18] and include viscoplastic fluids (e.g. Bingham model, Vocadlo model etc), thixotropic (time-dependent shear-thinning) fluids, rheopetic (anti-thixotropic) fluids, viscoelastic fluids (e.g. Oldroyd-B, FENE-P, PPT, Williamson, Maxwell etc) fluids and so on. Unfortunately these models although they include extra terms in the amended Navier-Stokes equations, the non-Newtonian models do not introduce length dependent effects which are associated with particles suspended in biofluids. These give rise to couple stresses which can exert a non-trivial influence on shear (and other) characteristics of physiological liquids. Stokes [19] introduced the "couple stress" fluid model in the mid-1960s to provide a framework for simulating biological and other industrial suspensions more precisely, by extending the conventional Cauchy stress. Couple stress or "polar" fluid models therefore are more elegant than the classical non-polar models. They also have the advantage that although they lead to boundary value problems with higher order than the Navier-Stokes, the supplementary terms are linear. This feature has stimulated considerable interest among engineers and applied physicists. Stokes [20] presented closed-form solutions for thermal conduction and convection in couple stress flows. Soundalgekar [21] investigated hydrodynamic solute dispersion in channel couple stress flows. Devakar et al. [22] considered couple stress fluid flows in several classical cases (Couette, Poiseuille and generalized Couette flow) observing that couple stresses decelerate the flow. Rammkissoon [23] conducted a detailed analytical study of drag effects in couple stress flow past a sphere using a Galerkin-type formulation and stream function due to a concentrated point force. Ramanaiah and Sarkar [24] used the polar model to analyse lubrication performance of infinitely long slider bearings, deriving expressions for load capacity, frictional force and centre of pressure and noting that greater couple stress effect enhances load capacity but decreases shear stress (wall frictional coefficient) i.e. induces deceleration. A number of biological couple stress flow models have also been communicated. These studies have considered peristaltic pumping in porous media [25], pulsatile blood flows [26], synovial tribology [27], stenotic hemodynamics with catheter and wall slip [28], micro-organism swimming dynamics [29], capillary transport with wall permeability [30,31] and mildly stenosed bifurcated arterial blood flow [32]. Excellent details of polar fluid dynamics are provided in Cowin [33] and more recently by Eringen [34].

Many physiological liquids are electrically-conducting owing to the presence of ions and iron content (e.g. haemoglobin in red blood cells). Such fluids are responsive to electrical and magnetic fields. Magnetohydrodynamic (MHD) pumping [35] has emerged as a robust mechanism for transporting such fluids in clinical applications (extra-corporeal surgical blood flow control). MHD pumps utilize the Lorentz effect which involves the injection of an electric current into two electrodes positioned at sidewalls facing each other in a micro-channel. This charge injection generates a transversal ionic current in the micro-channel which can be regulated by applied magnetic fields. The Lorentz force acting on the ionic current in the solution mobilizes a fluid flow in the micro-channel direction. Bi-directional pumping is also possible since flow reversal is induced by a reversal of the electric current or the magnetic field vector. Gastric flows may also be doped with magnetic particles to enable MHD endoscopy treatments. Several excellent studies of MHD pumping in medical engineering have been made which have included both theoretical and fabrication aspects. These include Zhong et al. [36] and Lim and Choo [37]. Recently Ponalagusamy and Selvi [38] simulated the magnetohydrodynamic blood flow in stenotic arterial flow with viscosity and peripheral plasma layer effects. Couple stress magnetohydrodynamic pumping flows have also received some attention. Tripathi and Bég [39] derived approximate solutions for velocity, pressure gradient, local wall shear stress and volumetric flow rate in hydromagnetic peristaltic pumping of couple stress fluids, considering both non-integral and integral numbers of waves. They highlighted the retarding effects of both couple stresses and magnetic field. Srinivasacharya and Rao [40] used a finite difference numerical method to compute the magnetized pulsating arterial couple stress blood flow, presenting extensive solutions for shear stress, flow rate and impedance near the apex, noting the significant deceleration by couple stresses in streaming blood flow near the lateral junction and

secondary flow damping by magnetic field near the apex in the daughter artery. Magnetic polar physiological hydrodynamic include periodic spinning blood magnetohydrodynamic separation device modelling was studied by Bég et al. [41]. Slip hydromagnetic couple stress flow in distensible channels was analyzed by El Shennawy and Elkhair [42]. Couple stress magnetic biological bearing tribology was simulated by Naduvinamani et al. [43] in which a Reynolds polar lubrication equation and the Christensen stochastic theory for roughness were used. Further studies include biothermodynamics of two-fluid couple stress liquids with thermal radiation for ablation therapy as examined by Murthy et al. [44] and thermo-magnetic Hall couple stress peristaltic pumping as reported by Hayat et al. [45]. Several researchers have also attempted to simulate ciliated magnetohydrodynamic flows. Siddiqui et al. [46] considered Newtonian channel flows and derived analytically the velocities, stream function and axial pressure gradient as a function of the cilia and metachronal wave velocity and also computed numerically the pressure rise per wavelength. They showed that trapping is reduced substantially with stronger magnetic field. Akbar et al. [47] used a viscoplastic fluid model to investigate hydromagnetic metachronal ciliated flow and heat transfer under an inclined magnetic field with wall slip and thermal jump effects. Akbar et al. [48] further investigated the ciliated propulsion of magnetized nanofluids using an elliptic beating cilia model. Bhatti et al. [49] have presented a theoretical study on the effects of magnetohydrodynamics on the peristaltic flow of Jeffrey fluid in a rectangular duct. Hayat et al. [50] have discussed the magnetohydrodynamic peristaltic motion based on the constitutive equations of a Carreau fluid in a channel. Saleem et al. [51] have constructed a mathematical model for MHD blood flow through an artery with mild stenosis. Saleem and Munawar [52] have studied the flow of blood through a stenotic artery in the presence of a uniform magnetic field. Ellahi et al. [53] have studied the peristaltic flow of a viscous fluid in a non-uniform rectangular duct. Bhatti et al. [54] have discussed the simultaneous effects of coagulation (blood clot) and variable magnetic field on peristaltically induced motion of non-Newtonian Jeffrey nanofluid containing gyrotactic microorganisms through an annulus. Bhatti et al. [55] have investigated the effects of variable magnetic field on peristaltic flow of Jeffrey fluid in a non-uniform rectangular duct having compliant walls.

In the current work a mathematical model is developed for hydromagnetic pumping of electrically-conducting couple stress physiological liquids (e.g. blood) through a two-dimensional ciliated channel under with metachronal waves generated by beating of the cilia. The Stokes' couple stress (polar) rheological model is employed. Closed-form solutions are developed for the problem under lubrication approximations and extensive computations are presented using MATLAB symbolic software for axial pressure gradient, axial (longitudinal) velocity, volumetric flow rate, wall shear stress function and pressure rise. Streamline visualization is also included to scrutinize bolus (trapping) phenomena. The study is relevant to MHD biomimetic blood pumps [36] and also may be of interest in simulating the hydrodynamics of micro-/nano-scale robots in biomedical devices [56].

2. Mathematical model

Consider the flow of an incompressible electrically-conducting couple stress non-Newtonian fluid through a symmetric channel with inner surfaces that are ciliated. We select Cartesian co-ordinates (X, Y), where the X-axis lies along the centre of the body and Y-axis is transverse to the fluid flow. The flow is generated due to a metachronal wave propagation which is produced by the collective, rhythmic beating of the cilia with constant wave speed c, along the channel walls. The schematic structure of the problem under consideration is depicted in Fig. 1. The geometry of the metachronal wave form proposes that the whip-like dynamics of the cilia may be simulated according to:

$$Y = f(X,t) = \pm\left[a + a\varepsilon\cos\left(\frac{2\pi}{\lambda}(X-ct)\right)\right] = \pm H \quad (1)$$

The experimental studies of Sleigh [57] confirm that the cilia tips move in elliptical paths. Therefore, the vertical position of the cilia tips can be written as:

$$X = g(X,t) = X_0 + a\varepsilon\alpha\sin\left(\frac{2\pi}{\lambda}(X-ct)\right) \quad (2)$$

Here a is the mean width, H is the semi-width of the channel, λ is the wavelength, t is time, α is the measure of the eccentricity, ε is the cilia length parameter and X_0 is indicated position of the particle. If the no slip hydrodynamic condition is imposed at the channel walls, then the velocities of the transporting fluid are merely those produced by the cilia tips, which can be given as:

$$U = \left.\frac{\partial X}{\partial t}\right|_{X_0} = \frac{\partial g}{\partial t} + \frac{\partial g}{\partial X}\frac{\partial X}{\partial t} = \frac{\partial g}{\partial t} + \frac{\partial g}{\partial X}U \quad (3)$$

$$V = \left.\frac{\partial Y}{\partial t}\right|_{X_0} = \frac{\partial f}{\partial t} + \frac{\partial f}{\partial X}\frac{\partial X}{\partial t} = \frac{\partial f}{\partial t} + \frac{\partial f}{\partial X}U \quad (4)$$

Invoking Eqs. (1) and (2) in Eqs. (3) and (4), readily yields the following expressions for the longitudinal velocity (U) and transverse velocity (V) components at the boundaries:

$$U = \frac{-\left(\frac{2\pi}{\lambda}\right)ac\varepsilon\alpha\cos\left(\frac{2\pi}{\lambda}(X-ct)\right)}{1-\left(\frac{2\pi}{\lambda}\right)a\varepsilon\alpha\cos\left(\frac{2\pi}{\lambda}(X-ct)\right)} \quad (5)$$

$$V = \frac{\left(\frac{2\pi}{\lambda}\right)ac\varepsilon\alpha\sin\left(\frac{2\pi}{\lambda}(X-ct)\right)}{1-\left(\frac{2\pi}{\lambda}\right)a\varepsilon\alpha\cos\left(\frac{2\pi}{\lambda}(X-ct)\right)} \quad (6)$$

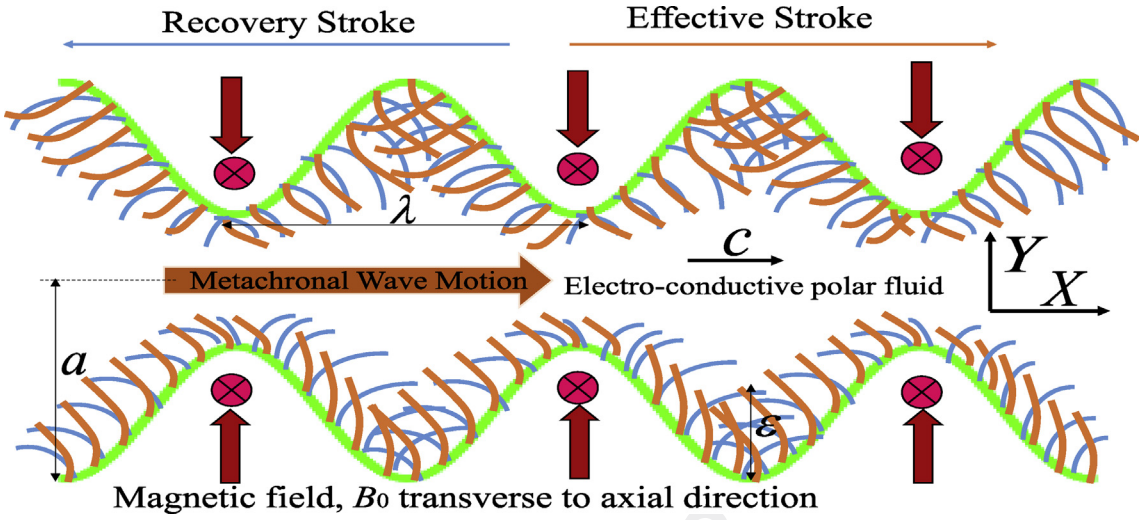

Fig. 1 Symmetric MHD metachronal wave propagation in a channel with ciliated walls.

In view of this formulation of the boundary conditions we are able to distinguish between the effective stroke of the cilia and the effective recovery stroke by approximately accounting for the shortening of the cilia. The governing equations for two-dimensional unsteady flow of an incompressible electrically-conducting couple stress (polar) fluids under the effect of a magnetic field applied transverse to the $X-Y$ plane (which generates two Lorentzian drag components in the X and Y directions respectively, viz $-\sigma B_0^2 U$ and $-\sigma B_0^2 V$) may be written as follows:

$$\frac{\partial U}{\partial X}+\frac{\partial V}{\partial Y}=0 \tag{7}$$

$$\rho\left(\frac{\partial U}{\partial t}+U\frac{\partial U}{\partial X}+V\frac{\partial U}{\partial Y}\right)=-\frac{\partial P}{\partial X}+\mu\left(\frac{\partial^2 U}{\partial X^2}+\frac{\partial^2 U}{\partial Y^2}\right)$$
$$-\eta\left(\frac{\partial^4 U}{\partial X^4}+2\frac{\partial^4 U}{\partial X^2\partial Y^2}+\frac{\partial^4 U}{\partial Y^4}\right)-\sigma B_0^2 U \tag{8}$$

$$\rho\left(\frac{\partial V}{\partial t}+U\frac{\partial V}{\partial X}+V\frac{\partial V}{\partial Y}\right)=-\frac{\partial P}{\partial Y}+\mu\left(\frac{\partial^2 V}{\partial X^2}+\frac{\partial^2 V}{\partial Y^2}\right)$$
$$-\eta\left(\frac{\partial^4 V}{\partial X^4}+2\frac{\partial^4 V}{\partial X^2\partial Y^2}+\frac{\partial^4 V}{\partial Y^4}\right)-\sigma B_0^2 U \tag{9}$$

Here $\frac{\partial P}{\partial X}$ is axial pressure gradient and $\frac{\partial P}{\partial Y}$ is transverse pressure gradient. To determine analytical solutions, it is advantageous to define the transformation between the laboratory (unsteady) frame and wave (steady) frame, for the present moving boundary value problem. The appropriate coordinate transformations are defined as:

$$x=X-ct, y=Y, u(x,y)=U(X,Y,t)-c$$
$$v(x,y)=V(X,Y,t), p(x,y)=p(X,Y,t) \tag{10}$$

Furthermore, we introduce the following non-dimensional parameters and hydrodynamic parameters:

$$\bar{x}=\frac{x}{\lambda}, \bar{y}=\frac{y}{a}, \bar{u}=\frac{u}{c}, \bar{v}=\frac{v}{c}, \bar{H}=\frac{H}{a}, \bar{t}=\frac{ct}{\lambda}$$
$$\bar{p}=\frac{a^2 p}{\lambda\mu c}, \beta=\frac{a}{\lambda}, Re=\frac{\rho c a}{\mu} \tag{11}$$
$$\gamma=\sqrt{\frac{\mu}{\eta}}a, M=\sqrt{\frac{\sigma}{\mu}}B_0 a$$

Where $\bar{x}$, $\bar{y}$, $\bar{u}$, $\bar{v}$, $\bar{H}$, $\bar{t}$, $\bar{p}$, β, Re, γ, M, denote non-dimensional axial coordinate, dimensionless transverse coordinate, non-dimensional axial velocity, dimensionless transverse velocity, dimensionless channel semi-width, dimensionless time, dimensionless pressure, wave number, Reynolds number, couple stress (polar) fluid parameter and Hartmann magnetic number, respectively. In the limit $\gamma\to\infty$, polar effects are neglected and the governing equations reduce to the classical Navier-Stokes equations for magnetohydrodynamic ciliated propulsion of a Newtonian fluid. Applying lubrication theory approximations i.e. long wavelength ($\beta << 1$) and low Reynolds number ($Re\to 0$) (i.e. Stokes flow) assumptions, implementing Eqs. (10) and (11) in Eqs. (1)–(9), after dropping the bars, the following linearized equations are generated:

$$\frac{\partial p}{\partial x}=\frac{\partial^2 u}{\partial y^2}-\frac{1}{\gamma^2}\frac{\partial^4 u}{\partial y^4}-M^2(u+1) \tag{12}$$

$$\frac{\partial p}{\partial y}=0 \tag{13}$$

$$\frac{\partial u}{\partial y}=0,\quad \frac{\partial^3 u}{\partial y^3}=0 \quad \text{at} \quad y=0 \tag{14}$$

The non-dimensional forms of the physical boundary conditions emerge as:

$$u = -1 - \frac{2\pi\varepsilon\alpha\beta\cos(2\pi x)}{1-2\pi\varepsilon\alpha\beta\cos(2\pi x)}$$
$$\frac{\partial^2 u}{\partial y^2} = 0 \quad \text{at} \quad y = h = 1 + \varepsilon\cos(2\pi x). \tag{15}$$

It is important to note here that couple stress fluids are much simpler than another group of microstructural non-Newtonian fluids i.e. micropolar fluids [58], since they possess no microstructure at the kinematic level and therefore the kinematics of such fluids is totally described using the velocity field i.e. angular velocity (micro-rotation) field is not required. The higher order gradient boundary conditions for axial velocity in Eqs. (14) and (15) are the so-called "stress-free conditions" which physically imply that couple stresses vanish at the channel wall inner surfaces.

The instantaneous volume flow rate in the fixed frame is given by

$$\Theta = \int_0^H U(X,Y,t)dY \tag{16}$$

The above expression in the wave frame becomes

$$q = \int_0^h u(x,y)dy \tag{17}$$

From Eqs. (10), (16) and (17), the expression for the volume flow rate can be written as

$$\Theta = q + ch \tag{18}$$

The time-mean flow over time period T at fixed position X is defined as

$$\overline{\Theta} = \frac{1}{T}\int_0^T \Theta dt \tag{19}$$

Using Eq. (18) into Eq. (19) and then integrating, yields

$$\overline{\Theta} = q + ac \tag{20}$$

Defining the dimensionless time-mean flows, Q and F, in the laboratory and wave frame, respectively, as

$$Q = \frac{\overline{\Theta}}{ac} \quad \text{and} \quad F = \frac{q}{ac} \tag{21}$$

From Eq. (20), the flow rate in the non-dimensional form can be written as follows:

$$Q = F + 1 \tag{22}$$

where. $F = \int_0^h u dy$

3. Analytical solutions

The normalized boundary value problem is well-posed and admits exact solutions. The closed-form solutions of Eqs. (12) and (13) subject to the dimensionless boundary conditions Eqs. (14) and (15) are obtained as:

$$u = \frac{1}{(m_2^2 - m_1^2)}\left(\frac{1}{1-2\pi\varepsilon\alpha\beta\cos(2\pi x)} - \frac{1}{M^2}\frac{dp}{dx} + \frac{1}{\gamma^2}\right)\left(\frac{m_1^2\cosh(m_2 y)}{\cosh(m_2 h)} - \frac{m_2^2\cosh(m_1 y)}{\cosh(m_1 h)}\right) - \frac{1}{M^2}\frac{dp}{dx} + \frac{1}{\gamma^2} \tag{23}$$

$$\frac{dp}{dx} = \frac{F - A_1}{A_2} \tag{24}$$

where,

$$m_1 = \sqrt{\frac{\gamma^2 + \gamma\sqrt{\gamma^2 - 4M^2}}{2}} \tag{25a}$$

$$m_2 = \sqrt{\frac{\gamma^2 - \gamma\sqrt{\gamma^2 - 4M^2}}{2}} \tag{25b}$$

$$A_1 = \frac{1}{(m_2^2 - m_1^2)}\left(\frac{1}{1-2\pi\varepsilon\alpha\beta\cos(2\pi x)} + \frac{1}{\gamma^2}\right)\left(\frac{m_1^2\sinh(m_2 h)}{m_2\cosh(m_2 h)} - \frac{m_2^2\sinh(m_1 h)}{m_1\cosh(m_1 h)}\right) + \frac{1}{\gamma^2} \tag{25c}$$

$$A_2 = -\frac{1}{M^2}\left(h + \frac{1}{(m_2^2 - m_1^2)}\left(\frac{m_1^2\sinh(m_2 h)}{m_2\cosh(m_2 h)} - \frac{m_2^2\sinh(m_1 h)}{m_1\cosh(m_1 h)}\right)\right) \tag{25d}$$

The dimensionless wall shear stress distribution for the present problem is given by

$$S_f = \frac{\partial u}{\partial y} - \frac{1}{\gamma^2}\frac{\partial^3 u}{\partial y^3} \tag{26}$$

$$S_f = \frac{m_1 m_2}{(m_2^2 - m_1^2)}\left(\frac{1}{1-2\pi\varepsilon\alpha\beta\cos(2\pi x)} - \frac{1}{M^2}\frac{dp}{dx} + \frac{1}{\gamma^2}\right)\left(\frac{m_1\sinh(m_2 y)}{\cosh(m_2 h)} - \frac{m_2\sinh(m_1 y)}{\cosh(m_1 h)} - \frac{m_1 m_2}{\gamma^2}\left(\frac{m_2\sinh(m_2 y)}{\cosh(m_2 h)} - \frac{m_1\sinh(m_1 y)}{\cosh(m_1 h)}\right)\right) \tag{27}$$

Upon substituting the Eq. (18) into Eq. (20), we obtain the solution for shear stress distribution as follows:

The non-dimensional pressure rise (Δp) is computed by the following expression:

$$\Delta p = \int_0^1 \left(\frac{dp}{dx}\right) dx \tag{28}$$

The stream function in the wave frame obeying the Cauchy-Riemann equations $\left(u = \frac{\partial \psi}{\partial y} \quad \text{and} \quad v = -\frac{\partial \psi}{\partial x} \right)$ may be computed by using Eq. (23). Numerical evaluation of the exact solutions is executed in MATLAB which permits a parametric assessment of the flow characteristics. Also visualization of streamlines is achieved with MATLAB software which allows an examination of bolus formation and trapping.

4. Computational results and interpretation

Selected computations for velocity, axial pressure gradient, shear stress and pressure rise characteristics, and also streamline distributions are illustrated in Figs. 2–7. Generally flow rate (Q) is prescribed as 2 and a relatively strong magnetic field is imposed (M is at least set to 2 in all the graphs, unless otherwise indicated, in consistency with actual MHD blood pump devices – see Zhong et al. [36] and Lim and Choi [37] wherein generally double the magnetic Lorentz force relative to the viscous hydrodynamic force is recommended). All data is provided in the captions.

Table 1 gives the comparison of velocity distribution for the present and earlier literature (Newtonian fluid). In the benchmark study of Ramesh [59], cilia effects were not considered, therefore in our model we have set ε (cilia length parameter) $= 0$, α (measure of the eccentricity) $= 0$, β (wave number) $= 0$, Q (ddimensionless time-mean flow in the laboratory frame) $= 1$, γ (couple stress (polar) fluid parameter) $\rightarrow \infty$ (i.e. Newtonian case) and M (Hartmann magnetic number) $\rightarrow 0$ (electrically non-conducting case i.e. vanishing magnetic field). Furthermore, porous medium and slip effects do not appear in our model and therefore data from Ramesh [59] which corresponds to the simplest case in that study (i.e. where the porous medium vanishes [infinite permeability] and there is no channel wall slip) is selected to ensure that the exact same conditions are enforced in both models. The legend used in Table 1 therefore is $\varepsilon = 0.5$, $\alpha = 0$, $\beta = 0$, $Q = 1$, $\gamma \rightarrow \infty$, $M \rightarrow 0$.It is evident that our results are in close agreement with that of Ramesh [59]. Confidence in the present analysis is therefore justifiably high.

Fig. 2(a)–(d) illustrate the evolution in axial velocity across the entire channel span ($-1.5 \leq y \leq +1.5$) for respectively a variation in metachronal wave number (β), cilia length (ε), couple stress parameter (γ) and magnetic field parameter (M). Generally with the exception of Fig. 2(c), different responses are induced in the core zone and the edge zones (near the ciliated walls). Increasing wave number (Fig. 2(a)) is found to accelerate the axial

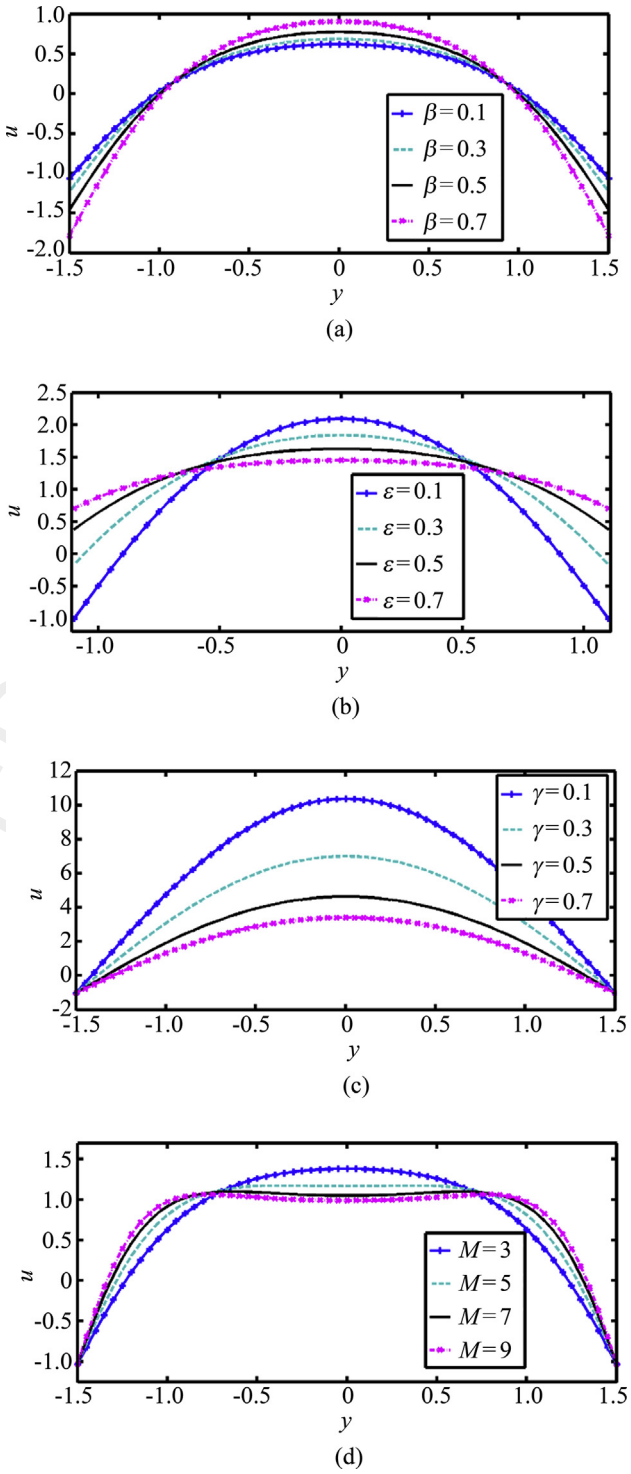

Fig. 2 Velocity profiles for different flow parameters for fixed values of. (a) $\varepsilon = 0.5$, $\alpha = 0.2$, $x = 1$, $Q = 2$, $\gamma = 3$, $M = 2.5$, (b) $\alpha = 0.1$, $\beta = 0.1$, $x = 1$, $Q = 2$, $\gamma = 2$, $M = 3$(c) $\varepsilon = 0.5$, $\alpha = 0.1$, $\beta = 0.1$, $x = 1$, $Q = 2$, $M = 3$, (d) $\varepsilon = 0.5$, $\alpha = 0.1$, $\beta = 0.1$, $x = 1$, $Q = 2$, $\gamma = 3$.

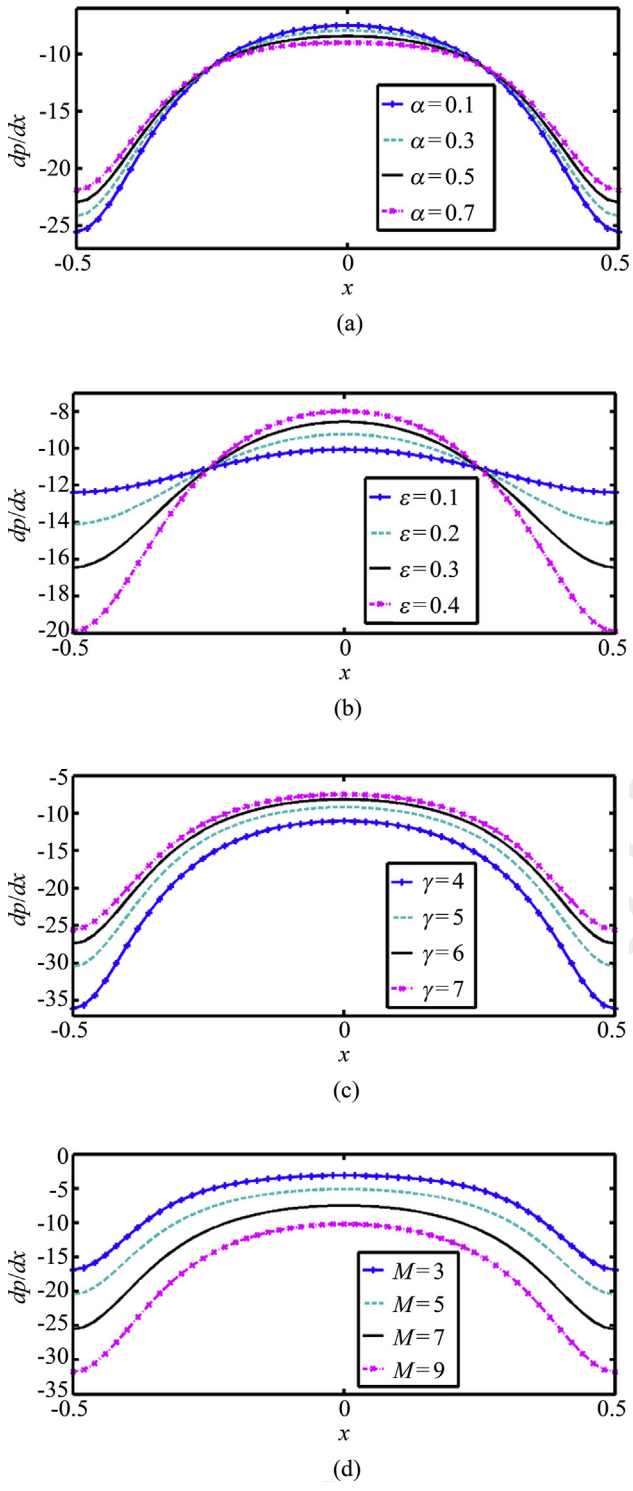

Fig. 3 Pressure gradient profiles for different flow parameters for fixed values of. (a) $\varepsilon=0.5$, $\beta=0.1$, $y=0$, $Q=1$, $\gamma=7$, $M=7$, (b) $\alpha=0.1$, $\beta=0.1$, $y=0$, $Q=1$, $\gamma=7$, $M=7$(c) $\varepsilon=0.5$, $\alpha=0.1$, $\beta=0.1$, $y=0$, $Q=1$, $M=7$, (d) $\varepsilon=0.5$, $\alpha=0.1$, $\beta=0.1$, $y=0$, $Q=1$, $\gamma=7$.

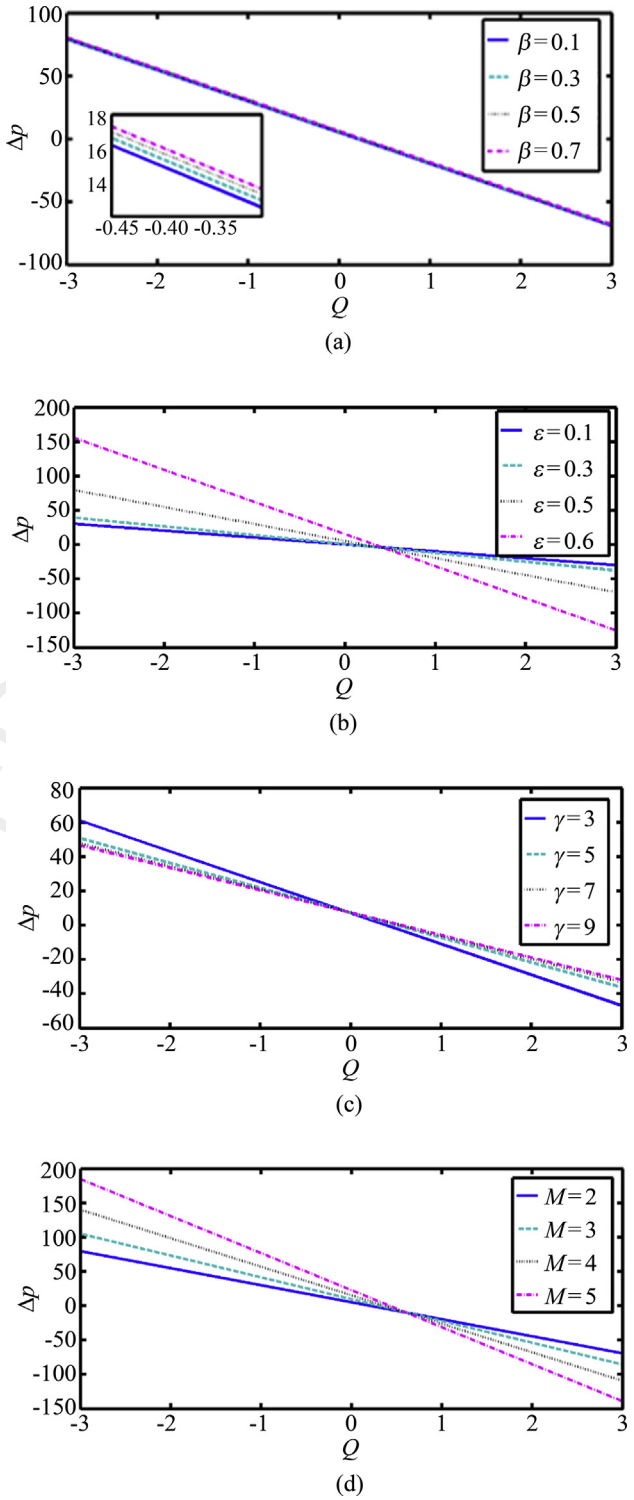

Fig. 4 Pressure rise profiles for different flow parameters for fixed values of. (a) $\varepsilon=0.5$, $\alpha=0.1$, $y=0$, $\gamma=2$, $M=2$, (b) $\alpha=0.1$, $\beta=0.1$, $y=0$, $\gamma=2$, $M=2$(c) $\varepsilon=0.5$, $\alpha=0.1$, $\beta=0.1$, $y=0$, $M=2$, (d) $\varepsilon=0.5$, $\alpha=0.1$, $\beta=0.1$, $y=0$, $\gamma=2$.

flow in the core zone but to decelerate it in the end zones. Peak axial velocity is computed logically at the channel centre line.

The parameter $\beta=\frac{a}{\lambda}$, where a is the mean width and λ is the wavelength of the metachronal wave. Clearly greater wavelengths reduce the wave number and vice versa for shorter wavelengths. In the channel core region, shorter

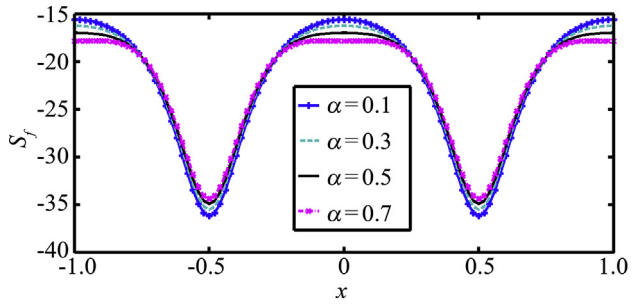

(a)

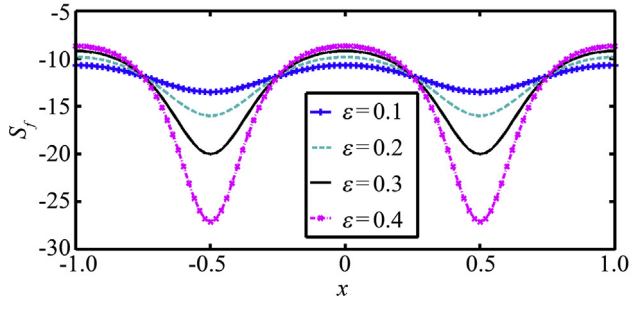

(b)

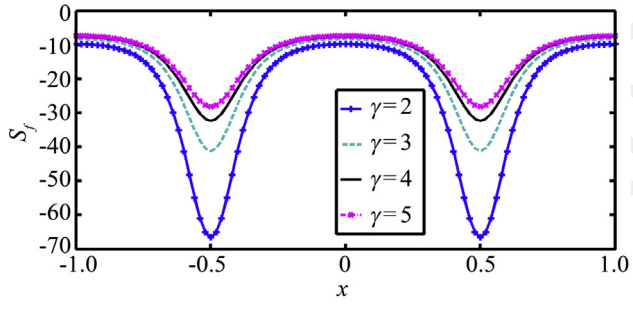

(c)

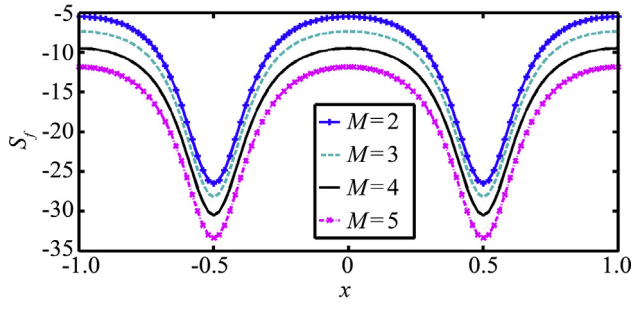

(d)

Fig. 5 Shear stress distribution for different flow parameters for fixed values of (a) $\varepsilon=0.5$, $\beta=0.1$, $Q=2, \gamma=7$, $M=7$, (b) $\alpha=0.1$, $\beta=0.1$, $Q=2, \gamma=3$, $M=3$(c) $\varepsilon=0.5$, $\alpha=0.1$, $\beta=0.1$, $Q=2, M=3$, (d) $\varepsilon=0.5$, $\alpha=0.1$, $\beta=0.1$, $Q=2, \gamma=5$.

wavelengths therefore result in acceleration whereas they induce deceleration in the proximity of the ciliated walls. The converse response is associated with larger wavelengths (smaller wave numbers). A similar observation for power-

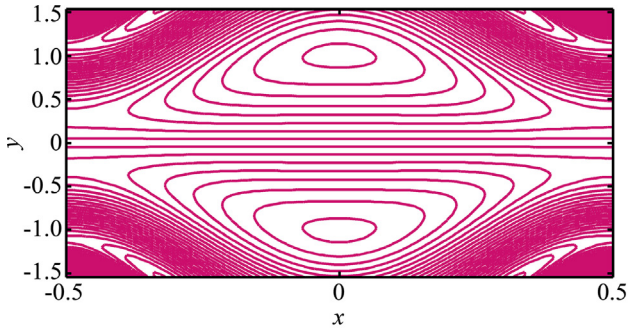

(a) $\beta=0$

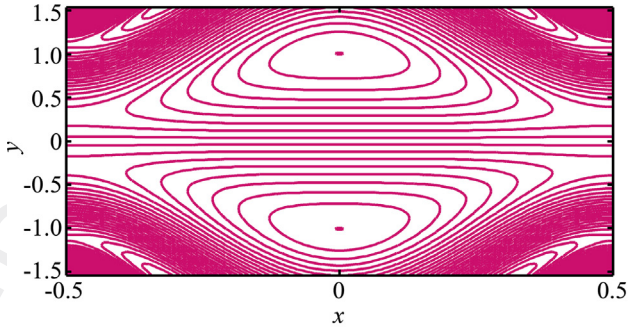

(b) $\beta=0.2$

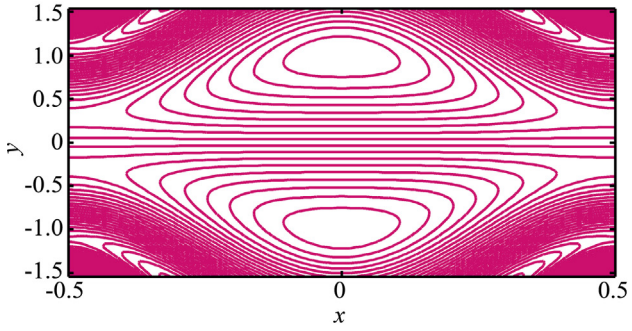

(c) $\beta=0.4$

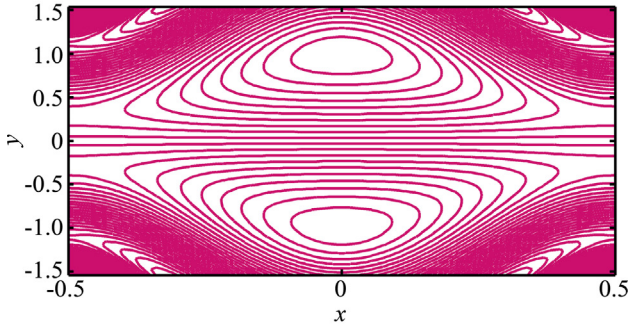

(d) $\beta=0.6$

Fig. 6 Streamline patterns for different values of wave number for fixed values of. $\varepsilon = 0.5$, $\alpha = 0.1$, $Q = 1, \gamma = 2$, $M = 2.5$

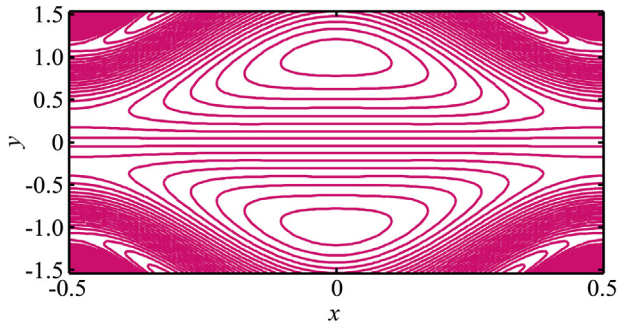

(a) $M=2.5$

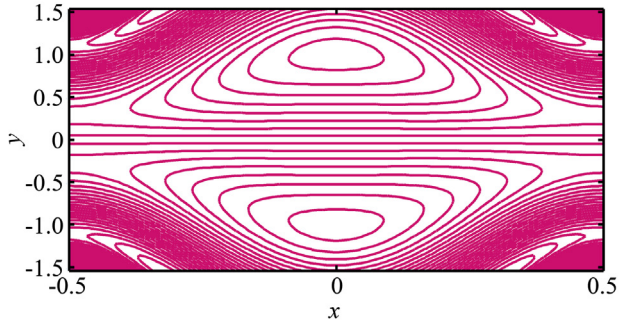

(b) $M=2.6$

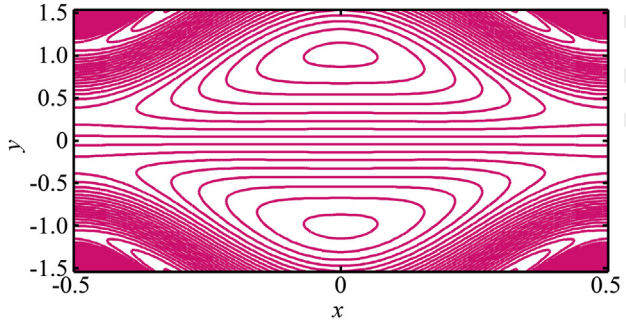

(c) $M=2.7$

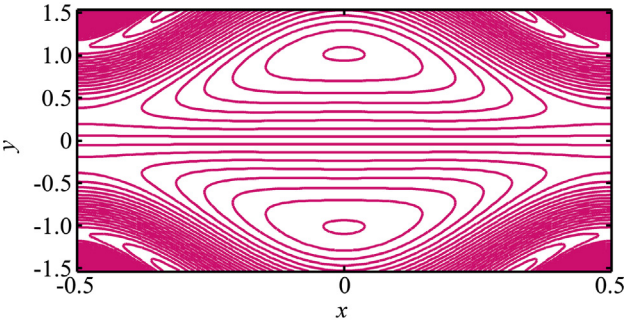

(d) $M=2.8$

Fig. 7 Streamline patterns for different values of Hartmann number for fixed values of. $\varepsilon = 0.5$, $\alpha = 0.1$, $Q = 1, \gamma = 2$, $\beta = 0.1$.

law and Newtonian fluids in ciliated channel wave propagation has been reported by Siddiqui et al. [60]. Fig. 2(b) shows that increasing cilia length induces a strong deceleration in the core region and also causes a substantial acceleration in the end zones (near wall regions). Clearly greater cilia length will offer more resistance to the axial flow which will impede pumping in the core region. The impact of cilia length is minimal at the walls since the protuberances exert a greater effect deeper into the channel. This manifests in a boost in axial velocity at the boundaries. Several studies have highlighted this including Sleigh [61] and more recently Khaderi et al. [62]. Elasticity of the cilia will also inevitably influence axial flow although this aspect has not been considered in the present work. It could be simulated in future by using a ratio between the viscous force and the elastic force in the cilia [62]. An increase in couple stress (polar) parameter, γ, as depicted in Fig. 2(c), is found to consistently decrease the axial velocity. The rise in γ, clearly leads to a reduction in the couple stress term in Eq. (12) $-\frac{1}{\gamma^2}\frac{\partial^4 u}{\partial y^4}$. The retarding nature of couple stresses as demonstrated in many other investigations [18–25] is confirmed by the present computations. Symmetry is sustained across the channel span in consistency with the wall boundary conditions. However very little flow reversal is induced compared with the near-wall axial flow field response in Fig. 2(a) and (b). Fig. 2(d) shows that an increase in magnetic body force parameter, M, stifles the bulk axial flow in the core zone but accelerates it towards the wall zones. This is a classical result from magnetohydrodynamics, confirmed in many standard works including Sutton and Sherman [63]. Significant backflow is induced close to both the lower and upper channel walls (approximately one third of the plots are below the zero line). Magnetic field is generally found to inhibit bulk flow of the couple stress fluid which is desirable in MHD pumping operations for enhanced flow control [36].

Fig. 3(a)–(d) present the response in axial pressure gradient (dp/dx) to alteration in cilia eccentricity parameter (α), cilia length (ε), couple stress parameter (γ) and magnetic field parameter (M) plotted against axial coordinate (channel length coordinate). An increase in eccentricity of the beating cilia induces a weak deceleration in the core flow and a corresponding acceleration in the edge flow, as illustrated in Fig. 3(a). The modifications in pressure gradient are more pronounced at the walls than in the core region. An increase in cilia length has a much more significant impact than cilia eccentricity, as plotted in Fig. 3(b). Considerable elevation is produced in the axial pressure gradient in the core zone with even greater depletion in axial pressure gradient in the end zones. Clearly the presence of longer elastic appendages (cilia) emanating from the walls interacts more intensively with the flow field than shorter cilia. There is never any skewness in the profiles which are all perfectly symmetric about the channel centre line. An increase in axial pressure gradient is generated with greater couple stress parameter (Fig. 3(c)) and once again this trend is enforced across the entire channel span. This enhancement in pressure gradient is physically consistent with the deceleration in axial flow computed earlier. Increasing magnetic field is also observed to diminish the axial pressure gradient, a characteristic feature of MHD pumps

Table 1 Comparison of velocity profile when.$\varepsilon = 0.5,\ \alpha = 0,\ \beta = 0,\ Q = 1,\ \gamma \to \infty,\ M \to 0$.

y	Newtonian fluid	Ramesh [59]	Present study
−1.5	−1.000000000000000	−0.999999999998181	−1.000000000000000
−1.2	−0.460000008344650	−0.460057371537914	−0.460063751198660
−0.9	−0.040000021457672	−0.040003307696679	−0.040008760610394
−0.6	0.260000005364418	0.260032609010523	0.260030306976534
−0.3	0.439999967813492	0.440053078913479	0.440053451562123
0	0.499999970197678	0.500059722193328	0.500062152979211
0.3	0.439999967813492	0.440053078913479	0.440053451562123
0.6	0.260000005364418	0.260032609010523	0.260030306976534
0.9	−0.040000021457672	−0.040003307696679	−0.040008760610394
1.2	−0.460000008344650	−0.460057371537914	−0.460063751198660
1.5	−1.000000000000000	−0.999999999998181	−1.000000000000000

[36,37]. This reduction is sustained across the entire channel i.e. there is no switch-over in profiles at the walls.

Fig. 4(a)−(d) illustrate the evolution of pressure rise (Δp) with volumetric flow rate (Q) with variation in respectively metachronal wave number (β), cilia length (ε), couple stress parameter (γ) and magnetic field parameter (M). The classical inverse relationship between pressure rise and volumetric flow rate (known for Newtonian fluids-see e.g. Wu [1] is also obtained for couple stress (polar) fluids for all plots. With increasing wave number (Fig. 4(a)), pressure rise is consistently decreased for all flow rates. However, with increasing cilia length (Fig. 4(b)), pressure rise is elevated in the pumping region ($\Delta p > 0$) whereas it is depressed in the augmented pumping region $\Delta p < 0$, with increasing flow rate. It is known that cilia spacing and length influences the viscous resistance per cilium and thereby the axial flow. The latter is assisted with greater cilia length and this aids in pressure rise in the lower channel half space (Fig. 4(b)). The introduction of extra energy to the flow at the lower wall however must be compensated for by an extraction at the upper wall, and these features are also related to synchronicity of beating cilia [2−10]. The pressure rise is therefore found to decrease with greater cilia length in the upper channel half space. The special case $\varepsilon = 0$ although not plotted implies vanishing cilia and absence of a metachronal wave - in this scenario the flow is a purely peristaltic mechanism due to flexibility of the walls. Maximum pressure rise therefore occurs for $\varepsilon = 0.6$, in the pumping region and the minimum pressure rise also corresponds to $\varepsilon = 0.6$, but in the augmented region. There is a significantly greater spread of linear decay profiles in Fig. 4(b) compared with the other plots. In the pumping region ($\Delta p > 0$), the pressure rise decreases with greater couple stress parameter (γ), whereas the opposite effect is induced in the augmented pumping region, as observed in Fig. 4(c). An increase in magnetic field parameter is conversely found to enhance pressure rise in the pumping region whereas it reduces pressure rise in the augmented pumping region, as shown in Fig. 4(d). In all the plots there exist also free pumping zones ($\Delta p = 0$) although this is essentially a cross-over point in Fig. 4(b)−(d). The impact of wave number on pressure difference is generally weak at all flow rates; however the cilia length, couple stress parameter and magnetic field impart a tangible modification to the pressure difference in the channel.

Fig. 5(a)−(d) present the shear stress distributions for various values of cilia eccentricity (α), cilia length (ε), couple stress parameter (γ) and magnetic field parameter (M). The oscillatory nature of shear (frictional wall force) is clearly captured and this is in synchrony with the metachronal beating of the cilia. Peaks and troughs are observed alternately in each of the plots. Increasing eccentricity ratio is found in Fig. 5(a) to considerably elevate the peak magnitudes of shearing stress but only weakly decrease the minimum values. More oblate topologies are also observed at the peaks compared with the troughs which are sharper. The shear stress direction is however never changed with a variation in eccentricity ratio (values are invariably negative) i.e. there is no flow reversal in the MHD pump channel. Fig. 5(b) indicates that peak shear stress values are mildly elevated with increasing cilia length whereas the troughs are very sharply decreased. The influence of cilia length is markedly greater than cilia eccentricity. Fig. 5(c) shows that with increasing couple stress parameter both the peaks and troughs are strongly reduced which is consistent with flow deceleration in polar fluids. In this plot there is also a weak flow reversal computed at low values of couple stress parameter, although this is quickly eliminated with higher values. Fig. 5(d) illustrates that increasing magnetic field similarly damps the shear stress strongly. The greater Lorentzian magnetic drag generated with higher M values retards the ciliated propulsion and the couple stress fluid shears therefore more slowly against the inner surfaces of the walls.

Finally in Fig. 6(a)−(d) and 7(a)−(d), MATLAB software has been used to plot streamline visualizations for the influence of two parameters, namely metachronal wave number (β) and magnetic field parameter (M), respectively. In both sets of plots the doubly symmetric dual bolus structure patterns are captured. With increasing metachronal wave number (β) i.e. decreasing wave length the central streamlines become increasingly distorted generating new bolus structures which grow symmetrically outwards into the channel space. Conversely with increasing magnetic parameter the newly

emerging bolus structures are contracted and vortex intensity is decreased in the channel. Trapping phenomena are therefore non-trivially influenced by both the metachronal wave length and applied magnetic field.

5. Conclusions

A theoretical investigation is presented for metachronal-wave generated propulsion of electro-conductive couple stress fluids in a channel with inner ciliated walls, motivated by simulating bio-inspired MHD pumps. The metachronal wave is aligned to the axial pumping direction and is simulated via an elliptical geometric model. Closed-form solutions for the transformed linearized boundary value problem are derived. Visualization of the analytical solutions is evaluated with symbolic software, MATLAB. The present computations have shown that:

- There is an inverse relationship between pressure rise and flow rate for variation in all geometric, material and magnetic control parameters.
- Increasing metachronal wave number elevates axial velocity in the core zone (whereas it induces axial flow retardation at the channel walls), generates decreasing pressure difference in the pumping and augmented pumping regions and encourages the growth of new secondary bolus structures in the channel.
- Increasing cilia eccentricity generates decreases axial pressure gradient in the core region (and increases it in the near-wall zones),
- Increasing cilia length decelerates the axial flow, increases the axial pressure gradient (in the core region), boosts pressure difference in the pumping region (positive pressures) and reduces it in the augmented pumping region (negative pressures) and furthermore weakly increases peak shear stresses and strongly reduces trough magnitudes.
- Increasing couple stress parameter retards the axial flow, elevates the axial pressure gradient across the full span of the channel, reduces pressure difference in the pumping zone, increases pressure difference in the augmented zone and enhances both peak and trough shear stress values.
- Increasing magnetic body force parameter decelerates the axial flow, reduces axial pressure gradient across the entire channel span, enhances pressure difference in the pumping zone, suppresses pressure difference in the augmented pumping zone, depresses both peak and trough shear stress values and mitigates the development of new bolus structures in the channel space.

Q2 The present study has presented a simple but interesting model for MHD physiological ciliated pumping systems. It has provided some useful benchmarks for further analysis which is presently being explored with ANSYS FLUENT computational fluid dynamics software. This will allow generalization to three-dimensional geometries and will also incorporation of elasticity of the ciliated structures. Efforts in this regard will be communicated in the near future.

References

[1] T.Y. Wu, Fluid mechanics of ciliary propulsion, in: Proc. Tenth Annual Meeting of the Society of Engineering Science, Yale University, Connecticut, USA, August, 1973.
[2] J. Kirch, M. Guenther, U.F. Schaefer, M. Schneider, C.M. Lehr, Computational fluid dynamics of nanoparticle disposition in the airways: mucus interactions and mucociliary clearance, Comput. Visual Sci. 14 (2011) 301−308.
[3] D. Chen, D. Norris, Y. Ventikos, Ciliary behaviour and mechano-transduction in the embryonic node: computational testing of hypotheses, Med. Eng. Phys. 33 (2011) 857−867.
[4] O.H. Shapiro, V.I. Fernandez, M. Garren, J.S. Guasto, F.P. Debaillon-Vesque, E. Kramarsky-Winter, A. Vardi, R. Stocker, Vortical ciliary flows actively enhance mass transport in reef corals, Proc. Natl. Acad. Sci. 111 (2014) 13391−13396.
[5] B. Siyahhan, V. Knobloch, D. de Zélicourt, M. Asgari, M. Schmid Daners, D. Poulikakos, V. Kurtcuoglu, Flow induced by ependymal cilia dominates near-wall cerebrospinal fluid dynamics in the lateral ventricles, J. R. Soc. Interface 11 (2014), 20131189.
[6] S. Gueron, K. Levit-Gurevich, Energetic considerations of ciliary beating and the advantage of metachronal coordination, Proc. Natl. Acad. Sci. 96 (1999) 12240−12245.
[7] B. Guirao, J.F. Joanny, Spontaneous creation of macroscopic flow and metachronal waves in an array of cilia, Biophys. J. 92 (2012) 1900−1917.
[8] A. Vilfan, F. Julicher, Hydrodynamic flow patterns and synchronization of beating cilia, Phys. Rev. Lett. 96 (5) (2006), 058102.
[9] I. Ibañez-Tallon, To beat or not to beat: roles of cilia in development and disease, Hum. Mol. Genet. 12 (2003) R27−R35.
[10] M. Brueckner, Cilia propel the embryo in the right direction, Am. J. Med. Genet. 101 (2011) 339−344.
[11] M.J. Lighthill, Flagellar hydrodynamics, SIAM Rev. 18 (2) (1975) 161−230.
[12] J. Elgeti, G. Gompper, Hydrodynamics of active mesoscopic systems, in: G. Munster, D. Wolf, M. Kremer (Eds.), NIC Symposium 2008, vol. 39, John von Neumann Institute for Computing, NIC Series, 2008, pp. 53−62.
[13] A. Dauptain, J. Favier, A. Bottaro, Hydrodynamics of Beating Cilia, IUTAM Symposium on Unsteady Separated Flows and Their Control, Corfu, Greece, 2007, pp. 18−22. June.
[14] A. Vilfan, F. Jülicher, Hydrodynamic flow patterns and synchronization of beating cilia, Phys. Rev. Lett. 96 (5) (2006), 058102.
[15] X.Z. Yang, R.H. Dillon, L.J. Fauci, An integrative computational model of multiciliary beating, Bull. Math. Biol. 70 (2008) 1192−1215.
[16] R.H. Dillon, L.J. Fauci, C. Omoto, Mathematical modeling of axoneme mechanics and fluid dynamics in ciliary and sperm motility, Dyn. Continuous Discrete Impuls. Syst. Ser. A - Math. Anal. 10 (5) (2002) 745−757.
[17] R. Dresdner, D. Katz, S. Berger, The propulsion by large amplitude waves of uniflagellar microorganisms of finite length, J. Fluid Mech. 97 (1980) 591−610.
[18] G.W. Scott Blair, Stock Image Introduction to Biorheology, Elsevier Science, New York, 1974.
[19] V.K. Stokes, Couple stresses in fluids, Phys. Fluids 9 (1966) 1709−1715.
[20] V.K. Stokes, On some effects of couple stresses in fluids on heat transfer, ASME J. Heat Transfer 91 (1969) 182−184.
[21] V.M. Soundalgekar, Effects of couple stresses in fluids on dispersion of a solute in a channel flows, Phys. Fluids 14 (1971) 19−20.
[22] M. Devakar, D. Sreenivasu, B. Shankarc, Analytical solutions of couple stress fluid flows with slip boundary conditions, Alexandria Eng. J. 53 (2014) 723−730.

[23] H. Rammkissoon, Drag in couple stress fluids, Z. Angew. Math. Phys. 29 (1978) 341–346.
[24] G. Ramanaiah, P. Sarkar, Slider bearings lubricated by fluids with couple stress, Wear 52 (1979) 27–36.
[25] A. Alsaedi, N. Ali, D. Tripathi, T. Hayat, Peristaltic flow of couple stress fluid through uniform porous medium, Appl. Math. Mech. 35 (2014) 469–480.
[26] P. Chaturani, D. Biswas, A comparative study of Poiseuille flow of a polar fluid under various boundary conditions with applications to blood flow, Rheol. Acta 23 (1984) 435–445.
[27] P.N. Tandon, S. Jaggi, A polar model for synovial fluid with reference to human joints, Int. J. Mech. Sci. 21 (1979) 161–169.
[28] J.V. Ramana Reddy, D. Srikanth, The polar fluid model for blood flow through a tapered artery with overlapping stenosis: effects of catheter and velocity slip, Appl. Bionics Biomechanics 2015 (2015), 174387.
[29] N. Ali, M. Sajid, Z. Abbas, O. Anwar Bég, Swimming of micro-organism in a fluid with couple stresses - a rheological model of embryological hydrodynamic propulsion, J. Mech. Med. Biol. 17 (3) 1750054 (23 pages).
[30] D. Pal, N. Rudraiah, R. Devanathan, A couple stress model of blood flow in the microcirculation, Bull. Math. Biol. 50 (1988) 329–344.
[31] J. Zueco, O. Anwar Bég, Network numerical simulation applied to pulsatile non-Newtonian flow through a channel with couple stress and wall mass flux effects, Int. J. Appl. Math. Mech. 5 (2) (2009) 1–16.
[32] D. Srinivasacharya, G.M. Rao, Mathematical model for blood flow through a bifurcated artery using couple stress fluid, Math. Biosci. 278 (2016) 37–47.
[33] S.C. Cowin, The theory of polar fluids, Adv. Appl. Mech. 14 (1974) 279–347.
[34] A.C. Eringen, Microcontinuum Field Theories, II: Fluent Media, Springer, New York, 2001.
[35] E.M. Korchevskii, L.S. Marochnik, Magnetohydrodynamic version of movement of blood, Biophysics 10 (1965) 411–413.
[36] J.H. Zhong, M.Q. Yi, H.H. Bau, Magnetohydrodynamic (MHD) pump fabricated with ceramic tapes, Sens. Actuators A Phys. 96 (2002) 59–66.
[37] S. Lim, B. Choi, A study on the MHD (magnetohydrodynamic) micropump with side-walled electrodes, J. Mech. Sci. Technol. 23 (2009) 739–749.
[38] R. Ponalagusamy, R. Tamil Selvi, Blood flow in stenosed arteries with radially variable viscosity, peripheral plasma layer thickness and magnetic field, Meccanica 48 (2013) 2427–2438.
[39] D. Tripathi, O. Anwar Bég, Transient magneto-peristaltic flow of couple stress biofluids: a magneto-hydro-dynamical study on digestive transport phenomena, Math. Biosci. 246 (2013) 72–83.
[40] D. Srinivasacharya, G. Madhava Rao, Computational analysis of magnetic effects on pulsatile flow of couple stress fluid through a bifurcated artery, Comput. Methods Progr. Biomed. 137 (2016) 269–279.
[41] O. Anwar Bég, S.K. Ghosh, S. Ahmed, T.A. Bég, Mathematical modelling of oscillatory magneto-convection of a couple stress bio-fluid in an inclined rotating channel, J. Mech. Med. Biol. (2012), Q3 121250050.1-1250050.35.
[42] R. El Shennawy, A. Elkhair, Lie point symmetries for a magneto couple stress fluid in a porous channel with expanding or contracting walls and slip boundary condition, Journal of the Egyptian Mathematical Society 24 (2016) 656–665.
[43] N.B. Naduvinamani, A. Siddangouda, S. Patil, Effect of surface roughness on static and dynamic characteristics of MHD couple stress lubrication of inclined plane slider bearing, ZAMM - Z. Angew. Math. Mech. (2017) 107–115. https://doi.org/10.1080/17515831.2017.1339485.
[44] J.V. Ramana Murthy, J. Srinivas, O. Anwar Bég, Entropy generation analysis of radiative heat transfer effects on channel flow of two immiscible couple stress fluids, J. Brazilian Soc. Mech Sci. Eng (2017), https://doi.org/10.1007/s40430-017-0752-6.
[45] T. Hayat, S. Asghar, A. Tanveer, A. Alsaedi, Effects of Hall current and ion-slip on the peristaltic motion of couple stress fluid with thermal deposition, Neural Comput. Appl. 31 (1) (2019) 117–126.
[46] A.M. Siddiqui, A.A. Farooq, M.A. Rana, Hydromagnetic flow of Newtonian fluid due to ciliary motion in a channel, Magnetohydrodynamics 50 (2014) 109–122.
[47] N.S. Akbar, D. Tripathi, O. Anwar Bég, Z.H. Khan, MHD dissipative flow and heat transfer of Casson fluids due to metachronal wave propulsion of beating cilia with thermal and velocity slip effects under an oblique magnetic field, Acta Astronaut. 128 (2016) 1–12.
[48] N.S. Akbar, Z.H. Khan, Influence of magnetic field for metachoronical beating of cilia for nanofluid with Newtonian heating, J. Magn. Magn. Mater. 381 (2015) 235–242.
[49] M.M. Bhatti, A. Riaz, R. Ellahi, Effects of magnetohydrodynamics on peristaltic flow of Jeffrey fluid in a rectangular duct through a porous medium, J. Porous Media 17 (2) (2014) 143–157.
[50] T. Hayat, N. Saleem, S. Mesloub, N. Ali, Magnetohydrodynamic flow of a Carreau fluid in a channel with different wave forms, Z. Naturforschung 66a (2011) 215–222.
[51] N. Saleem, T. Hayat, A. Alsaedi, A hydromagnetic mathematical model for blood flow of Carreau fluid, Int. J. Biomath. (IJB) 7 (2014), 1450010.
[52] N. Saleem, S. Munawar, A mathematical analysis of MHD blood flow of Eyring-Powell fluid through a constricted artery, Int. J. Biomath. (IJB) 9 (2016), 1650027.
[53] R. Ellahi, M.M. Bhatti, K. Vafai, Effects of heat and mass transfer on peristaltic flow in a nonuniform rectangular duct, Int. J. Heat Mass Transf. 71 (2014) 706–719.
[54] M.M. Bhatti, A. Zeeshan, R. Ellahi, Simultaneous effects of coagulation and variable magnetic field on peristaltically induced motion of Jeffrey nanofluid containing gyrotactic microorganism, Microvasc. Res. 110 (2017) 32–42.
[55] M.M. Bhatti, R. Ellahi, A. Zeeshan, Study of variable magnetic field on the peristaltic flow of Jeffrey fluid in a non-uniform rectangular duct having compliant walls, J. Mol. Liq. 222 (2016) 101–108.
[56] S. Palagi, Micro- and nanorobots in Newtonian and biological viscoelastic fluids, biologically inspired microscale robotic systems, in: Chapter 8, A Volume in Micro and Nano Technologies, 2017, pp. 133–162.
[57] M.A. Sleigh, The Biology of Cilia and Flagella, Mac Millan, New York, 1962.
[58] R. Bhargava, S. Sharma, O. Anwar Bég, J. Zueco, Finite element study of nonlinear two-dimensional deoxygenated biomagnetic micropolar flow, Commun. Nonlinear Sci. Numer. Simul. 15 (2010) 1210–1233.
[59] K. Ramesh, Effects of slip and convective conditions on the peristaltic flow of couple stress fluid in an asymmetric channel through porous medium, Comput. Methods Progr. Biomed. 135 (2016) 1–14.
[60] A.M. Siddiqui, T. Haroon, M. Rani, A.R. Ansari, An analysis of the flow of a power law fluid due to ciliary motion in an infinite channel, Biorheology 24 (2010) 56–69.
[61] M.A. Sleigh, Patterns of ciliary beating, in: Aspects of Cell Motility. Soc. Expl. Biol. Symp. XX II, Academic Press, New York, 1961.
[62] S.N. Khaderi, J.M.J. den Toonder, P.R. Onck, Fluid flow due to collective non-reciprocal motion of symmetrically-beating artificial cilia, Biomicrofluidics 6 (1) (2012), 014106-014106-14.
[63] G.W. Sutton, A.S. Sherman, Engineering Magnetohydrodynamics, MacGraw-Hill, New York, 1965.